

Epithermal Cu mineralization in the Stary Lesieniec rhyodacite quarry, Lower Silesia: primary and secondary mineral paragenesis

Stawomir MEDERSKI^{1, *}, Łukasz KRUSZEWSKI² and Jaroslav PRŠEK¹

¹ AGH University of Science and Technology, al. A. Mickiewicza 30, 30-059 Kraków, Poland

² Polish Academy of Sciences, Institute of Geological Sciences, Twarda 51/55, 00-818 Warszawa, Poland

Mederski, S., Kruszewski, Ł., Pršek, J., 2021. Epithermal Cu mineralization in the Stary Lesieniec rhyodacite quarry, Lower Silesia: primary and secondary mineral paragenesis. *Geological Quarterly*, 2021, 65: 43, doi: 10.7306/gq.1612

Associate Editor: Stanisław Z. Mikulski



Primary epithermal and secondary Cu mineralization in the Stary Lesieniec rhyodacite quarry, located within the Intra-Sudetic Depression, was studied using reflected light microscopy, powder X-ray diffraction, and electron microprobe. Samples containing copper sulphides, baryte, and secondary weathering minerals were collected from mineralized veinlets in the Upper Carboniferous rhyodacite. Copper sulphides (chalcocite Cu_2S , djurleite $\text{Cu}_{31}\text{S}_{16}$, anilite Cu_7S_4 /digenite Cu_9S_5 , and covellite CuS) are the major ore minerals and are associated with quartz, hematite, and very minor uraninite. The samples studied indicate phase transformation from chalcocite to anilite, which indicates that Cu sulphides began to crystallize at $\sim 100^\circ\text{C}$. Then, during the epithermal stage of precipitation, the temperature of the solutions dropped $< 72^\circ\text{C}$, based on the Cu-S ternary diagram and anilite stability. Admixtures of Ag, Fe, Bi, and Se in the sulphides are very minor. Supergene paragenesis is represented by chrysocolla with minor brochantite and very scarce malachite. These only bear trace impurities at the anionic sites. The supergene oxidation process began with the formation of abundant chrysocolla, at a relatively neutral pH. After dropping of the pH to $\sim 4\text{--}6$, brochantite was deposited.

Key words: Stary Lesieniec, copper sulphides, epithermal ore deposit, secondary minerals.

INTRODUCTION

Copper sulphides of the Cu-S system are the most common copper-bearing phases in many different genetic types of copper ore deposits, and are among the most important copper-bearing phases in the mining industry. They may form during primary-hydrothermal or secondary-weathering processes, usually at low or medium temperatures (e.g., Sillitoe and Clark, 1969; Hatert, 2005; Mathur et al., 2018). Primary chalcocite may crystallize as three main genetic types, under the following conditions: hypogene hydrothermal deposits ($> 150^\circ\text{C}$), red bed or stratiform deposits with circulating fluids through sedimentary basins ($< 150^\circ\text{C}$), or supergene enrichment ores that precipitate from low- to ambient-temperature oxidative fluids in near-surface environments (Mathur et al., 2018). The most common environment here is the cementation part of the supergene enrichment zone of various copper deposits – porphyry, SHMS (sediment-hosted massive sulphides), VHMS (volcanic-hosted massive sulphides), stratiform or hydrother-

mal types (Sillitoe and Clark, 1969; Gablina et al., 2006; Belogub et al., 2008; Mathur et al., 2018).

Minerals of the Cu-S system have a narrow field of stability in low-temperature conditions and they easily transform to each other during various natural processes (Goble, 1980; Goble and Robinson, 1981; Pósfai and Buseck, 1994). Usually, the formation of these Cu-sulphides starts with the crystallization of chalcocite and ends with covellite, at low temperatures. An experimental study producing transformation phase diagrams was described by Roseboom (1966) and followed up by Morimoto and Koto (1970), Cook (1972), Potter (1977), Evans (1981), together with equilibrium investigations by Schmidt et al. (1998).

Cu sulphide deposits in Poland are known within the Polish Kupferschiefer, where the minerals of Cu-S system are primary (mainly chalcocite, djurleite, more rarely covellite) or secondary (digenite, covellite) (Sawłowicz, 1990; Large et al., 1995; Pieczonka et al., 2007; Wodzicki and Piestrzyński, 2014; Mikulski et al., 2020; Szopa et al., 2021). They are also known from Miedzianka near Chęciny (Holy Cross Mts., central Poland), Miedzianka-Ciechanowice (Rudawy Janowickie Mountains, Sudetes, Lower Silesia), and from the Radzimowice deposits (Zimnoch, 1978; Wieser and Żabiński, 1986; Pieczka et al., 1988; Mikulski, 2005; Mochnacka et al., 2012). Copper mineralization within volcanic rocks is not so common in Poland. Examples include native copper with cuprite and secondary weathering copper minerals at Sokołowice (Siwe-

* Corresponding author, e-mail: mederski@agh.edu.pl

Received: May 25, 2021; accepted: August 9, 2021; first published online: September 14, 2021

cki, 2017), native copper in the Rudno and Nowy Kościół agates (Krawczyński, 1995; Dumańska-Słowik et al., 2008), chalcopyrite, chalcocite, covellite, and secondary weathering copper minerals at Zalas (Gołębiowska et al., 2006), and chalcopyrite and chalcocite at Borówno (Powolny et al., 2019). In addition, Cu mineralization hosted in baryte veins was described in Zagórze Śląskie, where chalcopyrite is associated with secondary malachite (Piestrzyński and Kowalik, 2015) and at Przygórze, near Nowa Ruda, where Cu ore comprising simple Cu sulphides (chalcocite, with minor chalcopyrite and possible geerite and roxbyite) disseminated in (carbonate-bearing) baryte veins is weathered, exclusively, to slightly magnesian malachite, $\text{Cu}_2(\text{CO}_3)(\text{OH})_2$ (Kruszewski et al., 2019). Similar hydrothermal copper mineralization (with chalcopyrite, bornite, native copper, chalcocite, and other copper sulphides) has been described from various localities worldwide and is mostly connected with volcanic rocks (Rojkovič, 1990; Rojkovič et al., 1993; Ferenc and Rojkovič, 2001; Emetz et al., 2006; Cabral and Beaudouin, 2007; Konari et al., 2013; Németh et al., 2017; Vlasáč et al., 2018; Kettanah, 2019; Palyanova et al., 2020; and others).

Among the currently (May 2021) 5704 approved mineral species, there are a great abundance of secondary weathering copper minerals. Formed due to weathering of the primary minerals, the final chemical composition, and mineralogical complexity of their assemblages is dependent on the interaction of the weathering products with elements and ions contained in both the country rock and solutions derived, e.g., from meteoric waters. The most common deposits with a broad range of secondary copper minerals are the Miedzianka and Radzimowice localities (Wieser and Žabiński, 1986; Pieczka et al., 1988; Siuda and Kruszewski, 2006, 2013; Siuda and Gołębiowska, 2011; Swęd et al., 2015; Parafinuk et al., 2016).

This study describes the mineralogy and phase transitions in low-temperature epithermal copper-baryte mineralization with secondary phases identified in a rhyodacite quarry at Stary Lesieniec. Both primary and secondary mineralogy is addressed here.

LOCALITY AND GEOLOGICAL SETTING

The Stary Lesieniec rhyodacite quarry is located within the administrative boundaries of the western part of the town of Boguszów Gorce, ~8 km west of Wałbrzych and ~1 km southwest of Mniszek Hill. The quarry is situated within the Wałbrzych Depression, which is part of the Intra-Sudetic Basin (ISB). The 70 km long and 35 km wide ISB is located at the NE margin of the Bohemian Massif (Holub, 1976; Lorenz and Nicholls, 1976; Wojewoda and Mastalerz, 1989; Awdankiewicz et al., 2003). The structure is filled with a lower Carboniferous to upper Permian molasse succession, comprising various Carboniferous and Permian volcanogenic rocks with common interbeds of sedimentary and tuffogenous deposits. Volcanogenic rocks are linked to a post-collisional extension-related setting in transition to a within-plate setting (Awdankiewicz, 1998, 1999; Mikulski and Williams, 2014) and result from subsequent Early Permian magmatic activity (Kozłowski, 1958, 1963).

The rhyodacites form a sheet-like, conformable body, up to 200 m thick in the eastern-central part, and wedge out west- and southwards (Fig. 1). The volcanic body is underlain by the topmost deposits of the Żacleń Formation (Westphalian B/C) and is overlain by the Ludwikowice Formation (Upper Stephanian). In addition, the SE part of the rhyodacites occurs within the Glinik Formation (Westphalian/Stephanian). According to Awdankiewicz (1999), the rhyodacites are most probably of extrusive origin (Grocholski, 1965; Nemeč, 1979). The rhyodacite, which is phenocryst-rich, is characterized by the presence of columnar joints perpendicular to the margins of the rock body (Awdankiewicz, 1999). Some of these columnar joints, occurring within the western wall of the quarry, are filled with epithermal Cu mineralization, which is the subject of this study.

MATERIALS AND METHODS

Samples of mineralized rocks were collected from the western part of the quarry (50°45'17" N, 16°10'17" E). The samples

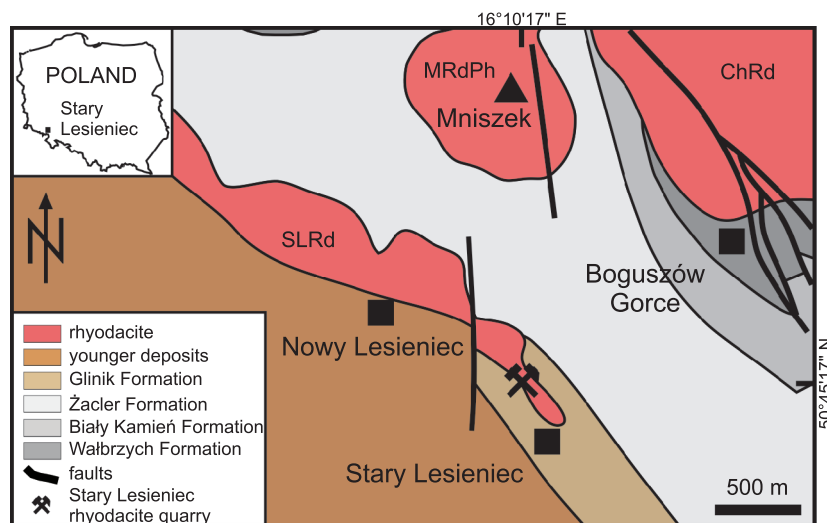


Fig. 1. Simplified geological map of the Stary Lesieniec area

SLRd – Stary Lesieniec rhyodacites, ChRd – Chelmiec rhodacites, MRdPh – Mniszek rhyodacite phacolith (modified from Grocholski, 1973; Awdankiewicz, 1999)

were carefully checked macroscopically and selected for further microscopic and Powder X-Ray Diffraction (PXRD) studies, as well as microprobe analysis.

The samples were ground in agate mortar and analysed using PXRD method for phase and structural analysis. A Bruker axis *D8 ADVANCE* diffractometer, equipped with VANTEC-1 superfast linear position-sensitive detector (LPSD), CoK α radiation source ($k\beta$ -filtered), with no monochromator, was used.

An increment of 0.02 2θ was used with 1s/step (~416 s/step in the LPSD language), and the samples were exposed in the 3–80 2θ range. For the structural analysis (i.e., unit cell parameters calculation), the PXRD data were modelled using the Rietveld refinement method (Rietveld, 1967) implemented in *TOPAS v. 4.0* software. In quantitative phase analysis (QPA) of the sample, in the case of chrysocolla (lacking structural model), the input data were introduced as a hkl phase (Pawley method, Pawley, 1980). The refinement procedure was controlled, i.e., by the attendance of one of us (Ł.K.) in the Reynolds Cup 2018 competition. Details of the refinement approach are described in Kruszewski (2013).

The chemical composition of the primary minerals was studied by EPMA, using the *JEOL Super Probe 8230* in the Laboratory of Critical Elements at the Faculty of Geology, Geophysics and Environmental Protection, AGH-UST, Kraków. The following operating conditions and standards were used: accelerating voltage 20 kV, beam current 20 nA, and a beam diameter of 5 μm . The following wavelengths (to omit interferences between the elements' spectral lines) were used: ZnK α , CuK α , SK α , FeK α , AgL α , AsL α , SbL α , BiM α , SeL α . Natural mineral standards (FeS₂, ZnS, PbS) and synthetic compounds (Sb₂S₃, Cu, Ag, Bi, Se) were used for calibration. All interferences between the element spectral lines were calculated using autocorrections based on standards. The detection limits for elements analyses in the Cu sulphides were as follows: S – 0.01 wt.%, Cu – 0.025 wt.%, As – 0.03 wt.%, Sb – 0.02 wt.%, Bi – 0.05 wt.%, Ag – 0.02 wt.%, Zn – 0.03 wt.%, Fe – 0.01 wt.%, Se – 0.075 wt.%.

The chemical composition of the secondary minerals was also studied by EPMA, using a *Cameca SX100* microprobe located in the Inter-Institution Laboratory of Microanalysis of Minerals and Synthetic Substances, Institute of Geochemistry, Mineralogy and Petrology, Faculty of Geology, University of Warsaw. A standard 15 keV current was used. Two other current parameters – amperage and beam size – and their influence on the wt.% values were tested before establishing the fi-

nal ones: 5 nA and 10 μm for chrysocolla (and similar silicates); 10 nA and 5 μm for brochantite and malachite. The following standards were used: diopside (Si, Mg, Ca), orthoclase (Al, K), cuprite (Cu), sphalerite (Zn), Fe₂O₃ (Fe), rhodonite (Mn), baryte (S), tugtupite (Cl), rutile (Ti), YPO₄ (P), and V₂O₅ (V). Due to possible interferences, Na presence and line coincidence was tested via WDS scanning; Na presence was not confirmed in the minerals studied. The reported wt.% are not normalized, as will be explained below.

RESULTS

Samples of the mineralized veinlets were taken from the western walls of the quarry, at the lower mining level (Fig. 2). This mineralization filled columnar joints, the parameters of which are as follows: dip direction: 56–83°, dip angle: 60–77°.

PRIMARY MINERALS

Copper sulphides (chalcocite Cu₂S, djurleite Cu₃₁S₁₆, anilite Cu₇S₄/digenite Cu₆S₅, and covellite CuS) are the major ore minerals and are associated with baryte, quartz, and secondary minerals in small veinlets (up to 10 cm width). The best QPA model for the ore sample is obtained when low-temperature, trigonal digenite is included. However, the results are very similar to those obtained in a digenite-free model. The ore composition is (in wt.%): 69.6(7) low-temperature chalcocite, 7.3(7) anilite, 6.23(8) djurleite, and 0.223(7) digenite, with the remainder of 16.8(5) being baryte ($R_{wp} = 8.46\%$, GOF = 1.63%, DW = 0.78%, where: R_{wp} is the residual weighted-pattern, GOF is goodness of fit also known as χ^2 , and DW is Durbin-Watson statistics). Minerals related to sulphide paragenesis differ in Cu/S ratio (Fig. 3) and do not show significant enrichment in the trace elements (TEs) measured. The content of individual TEs is not dependent on sulphide species systematics. The Ag concentration in the sulphides reaches up to 0.18 wt.%; Bi – up to 0.16 wt.%; Se – up to 0.19 wt.%; and Fe – up to 0.03 wt.% respectively.

Chalcocite is the dominant mineral phase in sulphide intergrowths and forms aggregates up to few centimetres in diameter (Fig. 4A–D). It is characterized by a blue-grey colour and weak anisotropy. The generalized chalcocite formula based on

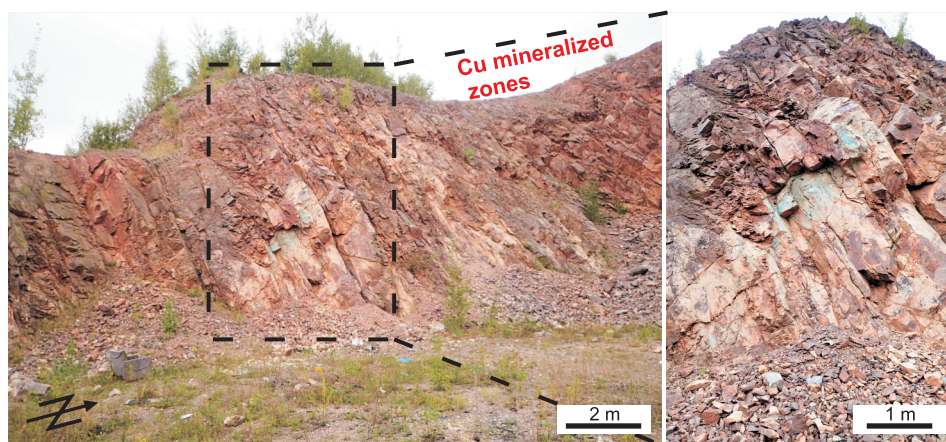


Fig. 2. Field images from the Stary Lesieniec rhyodacite quarry

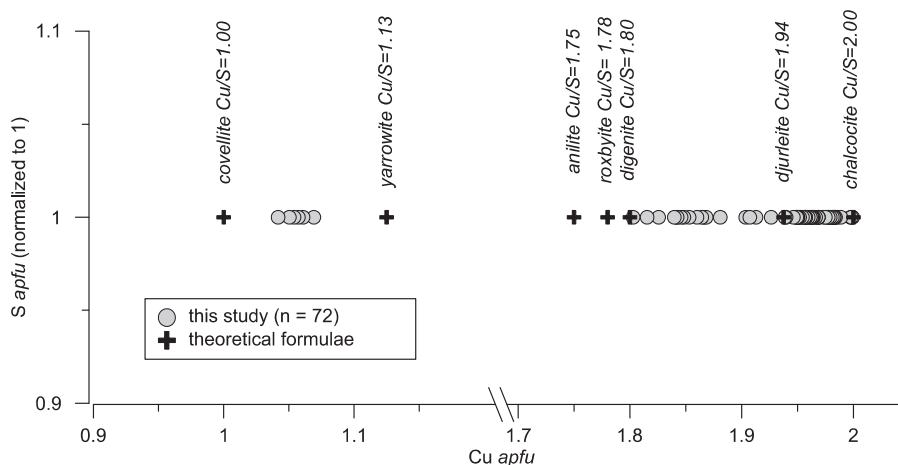


Fig. 3. Chemical composition of copper sulphides from the Stary Lesieniec rhyodacite quarry

1 anion is $\text{Cu}_{1.96-2.00}\text{S}_{1.00}$ (Appendix 1*, analyses 1–8). The Cu/S ratio is 1.96–2.00 (Fig. 3). Most of the values are very close to the ideal Cu/S ones (2.00). The unit cell parameters of the chalcocite are: $a = 15.279(1)\text{\AA}$, $b = 11.77(1)$, $c = 13.488(9)\text{\AA}$, and $\beta = 116.85(5)^\circ$.

In the samples studied, **djurleite** is less prevalent. It shows weak anisotropy, a bluish-grey colour, and a lower reflectance as compared to the chalcocite. It usually forms irregular intergrowths in chalcocite aggregates (Fig. 4C, D). Djurleite is either synchronous with or younger than the chalcocite. The generalized empirical djurleite formula based on 16 anions is: $(\text{Cu}_{30.46-31.38}\text{Ag}_{0.01-0.03}\text{Bi}_{0.00-0.02}\text{Fe}_{0.00-0.01})_{\Sigma 30.51-31.42}(\text{S}_{15.95-16.00}\text{Se}_{0.00-0.05})_{\Sigma 16.00}$ (Appendix 1, analyses 9–14), while the Cu/S ratio is 1.93–1.96 (Fig. 3). A lot of the Cu/S values are very close to the ideal ones (1.94). The PXRD pattern of the djurleite was indexed on a monoclinic unit-cell, with $a = 28.65(9)\text{\AA}$, $b = 15.637(6)\text{\AA}$, $c = 13.43(4)\text{\AA}$, and $\beta = 89.23(25)^\circ$.

Anilite/digenite forms elongated lamellae, up to 1 mm long, along the cleavage planes in older Cu sulphides (Fig. 4A, C, D). It is more commonly found within chalcocite crystals (Fig. 4A, C) than in djurleite (Fig. 4D). Anilite/digenite are characterized by a distinctly light blue colour and significantly lower reflectance than the previously mentioned sulphides. The generalized formula based on 5 anions can be expressed as $(\text{Cu}_{9.01-9.40}\text{Ag}_{0.01})_{\Sigma 9.02-9.42}(\text{S}_{4.99-5.00}\text{Se}_{0.00-0.01})_{\Sigma 5.00}$ (Appendix 1, analyses 15–18). The Cu/S ratio is 1.81–1.88 (Fig. 3), which suggests a chemical composition closer to digenite. On the other hand, the amount of anilite outweighs the amount of digenite, as shown by QPA. The content of the particular species is thus likely very variable among the mineralized zone. The unit cell parameters of anilite are $a = 7.928(7)\text{\AA}$, $b = 7.78(3)\text{\AA}$, and $c = 10.97(1)\text{\AA}$; those of digenite are as follows: $a = 16.50(5)\text{\AA}$, $c = 14.28(19)\text{\AA}$.

Fractures cross-cutting older sulphide masses and contacts between chalcocite and djurleite are often filled with secondary **covellite** (Fig. 4D). This is characterized by the typical indigo-blue colour, strong birefractance, and strong, pinkish to orange, anisotropy. It should be mentioned that within the veinlets there are non-cracked, fresh sulphide zones, and zones with a higher proportion of brecciation bearing covellites and other

secondary phases. The generalized covellite formula based on 1 anion is $\text{Cu}_{1.04-1.07}\text{S}_{1.00}$ (Appendix 1, analyses 19, 20). The Cu/S ratio in covellite varies from 1.04 to 1.07, which indicates a higher copper content and transitional chemical character, being intermediate between covellite and yarrowite (Fig. 3).

Baryte form irregular masses as well as idiomorphic crystals up to 2 mm long between chrysocolla and rhyodacite clasts (Fig. 4E). The voids within the baryte are usually filled with chrysocolla. Finally, the parameters of the baryte are $a = 8.866(4)\text{\AA}$, $b = 5.447(3)\text{\AA}$, and $c = 7.148(3)\text{\AA}$. The related statistical parameters are: $R_{wp} = 7.69\%$, $\text{GOF} = 1.55\%$, $\text{DW} = 0.87\%$. The baryte crystals are characterized by the presence of numerous fluid inclusions, as well as fibrous **hematite** aggregates (Fig. 4F).

Quartz occurs as idiomorphic crystals with diameters up to 100 μm , which intersects Cu sulphide aggregates as well as baryte crystals.

As many as 3 larger inclusions of an U-O phase were detected within a single microarea of chrysocolla (Fig. 5D). In addition, one larger crystal was observed in a chalcocite aggregate (Fig. 4B). Only two analyses were possible, with the following wt.% contents: P_2O_5 : 0.00, 0.45; SiO_2 : 2.62, 6.46; UO_2 : 84.27, 77.39; Al_2O_3 : 0.09, 0.57; CuO : 5.90, 4.64; PbO : 1.43, 0.00; MnO : 0.00, 0.66; CaO : 3.17, 4.06; K_2O : 0.00, 0.24; with totals of 97.48 and 94.47, respectively, and S, Th, Zr, Ti, Fe, and Mg oxides were below their detection limits. After deducing the largely variable Si contents, and also Cu and Al contents as interferences from the matrix, the analyses recasted with a 4-cation basis give the mean formula of $(\text{U}^{4+}_{0.80}\text{Ca}_{0.18}\text{Mn}_{0.01}\text{Pb}_{0.01})_{\Sigma 1.00}\text{O}_{1.80}$. The lowered calculated O amount suggests the mineral to be the “pitchblende” variety, U_3O_8 . A re-recasted analysis, based on the suggested average U valency of 5.775 (Estep, 2012), gives the formula $(\text{U}_{2.40}\text{Ca}_{0.53}\text{Mn}_{0.04}\text{Pb}_{0.03}\text{P}_{0.01})_{\Sigma 1.00}\text{O}_{7.56}$.

SECONDARY MINERALS

Chrysocolla, $\text{Cu}_{2-x}\text{Al}_x(\text{H}_{2-x}\text{Si}_2\text{O}_5)(\text{OH})_4 \cdot n\text{H}_2\text{O}$ ($x < 1$), and/or its amorphous precursor is the major secondary Cu species in

* Supplementary data associated with this article can be found, in the online version, at doi: 10.7306/gq.1612

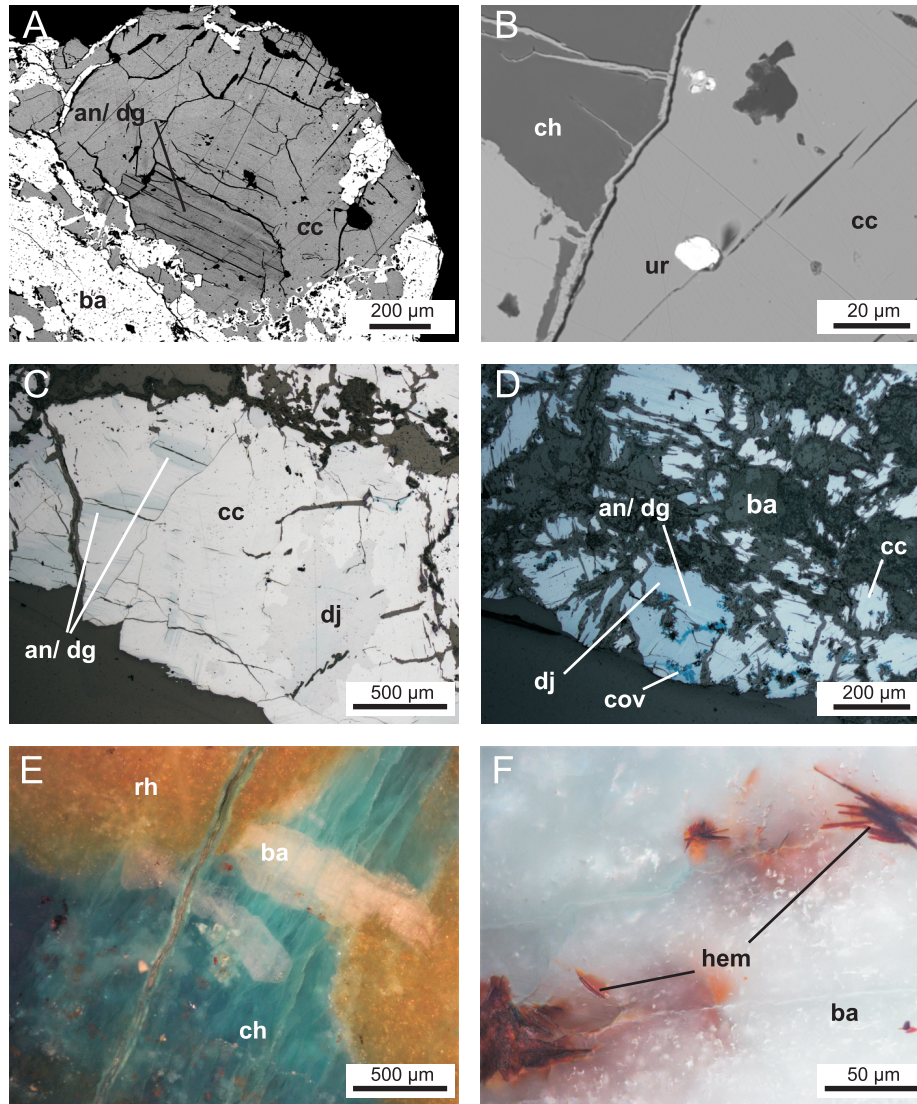


Fig. 4. Back-Scattered-Electron (BSE) images (A, B), optical [reflected light, 1P (C, D); 2P (E, F)] illustrating the primary assemblage from Stary Lesieniec

A – chalcocite (cc) with elongated anilite/digenite (an/dg) lamellae along the cleavage planes surrounded by younger baryte (ba); **B** – idiomorphic uraninite (ur) crystal in chalcocite; chrysocolla (ch); **C** – chalcocite with irregular djurleite (dj) zones and younger elongated anilite/digenite lamellae; **D** – disintegrated chalcocite–djurleite–anilite/digenite aggregates with secondary covellite (cov) veinlets; **E** – idiomorphic baryte crystals between rhyodacite (rh) clasts surrounded by chrysocolla (ch); **F** – fibrous hematite (hem) crystals in baryte

the material studied. Most chrysocolla aggregates are massive and vivid blue, with some sharp outlines of a crystalline predecessor observed only locally (Fig. 5A, C, D). The bluish-white variety of chrysocolla is rare. The chrysocolla is locally covered by very tiny (<1 mm long) bright green, chaotically intergrown needles of brochantite, $\text{Cu}_4(\text{SO}_4)(\text{OH})_6$ (Fig. 5B). Its typical, high-lustre, flat lamellar crystals are also observed locally, covering the baryte (Fig. 5E), but this type of habit is rare. **Malachite**, $\text{Cu}_2(\text{CO}_3)(\text{OH})_2$ was only detected in tiny amounts in a single sample, covering the baryte. It is difficult to macroscopically distinguish from **brochantite** due to its tiny size. The identity of black specks of a massive substance very locally covering the chrysocolla could not be determined via the PXRD, presumably both to their low volume and low crystallinity. However, black, typically dendritic “wad”, covering rocks in the outer part

of the exposure was shown by hand-held X-Ray Fluorescence Spectroscopy (pXRF) to be, indeed, a Mn-(hydr)oxide, bearing essential admixtures of Cu, Ni, and Co. Vanadium was often seen in some pXRF spectra but this find is not well-founded in the EPMA study which did not allow detection of this element in any of the primary and secondary minerals analysed. It is thus suspected that V occurs in the rock matrix.

Only a single sample studied by PXRD has shown a few reflections attributable to chrysocolla, at $d = 1.467$ (very broad) 2.876 and 4.421 Å (both broad), with the one at 17.16 Å being very diffuse and low in its intensity. The calculated unit cell parameters are: $a = 5.799(6)\text{Å}$, $b = 17.64(1)\text{Å}$, $c = 8.081(7)\text{Å}$ ($R_{\text{wp}} = 4.72\%$, $\text{GOF} = 1.42\%$, $\text{DW} = 1.02\%$). Parameters obtained for brochantite are $a = 13.096(6)\text{Å}$, $b = 9.868(4)\text{Å}$, $c = 6.022(2)\text{Å}$, and $\beta = 102.93(7)^\circ$ ($R_{\text{wp}} = 9.18\%$, $\text{GOF} = 1.54\%$, $\text{DW} = 0.90$) for

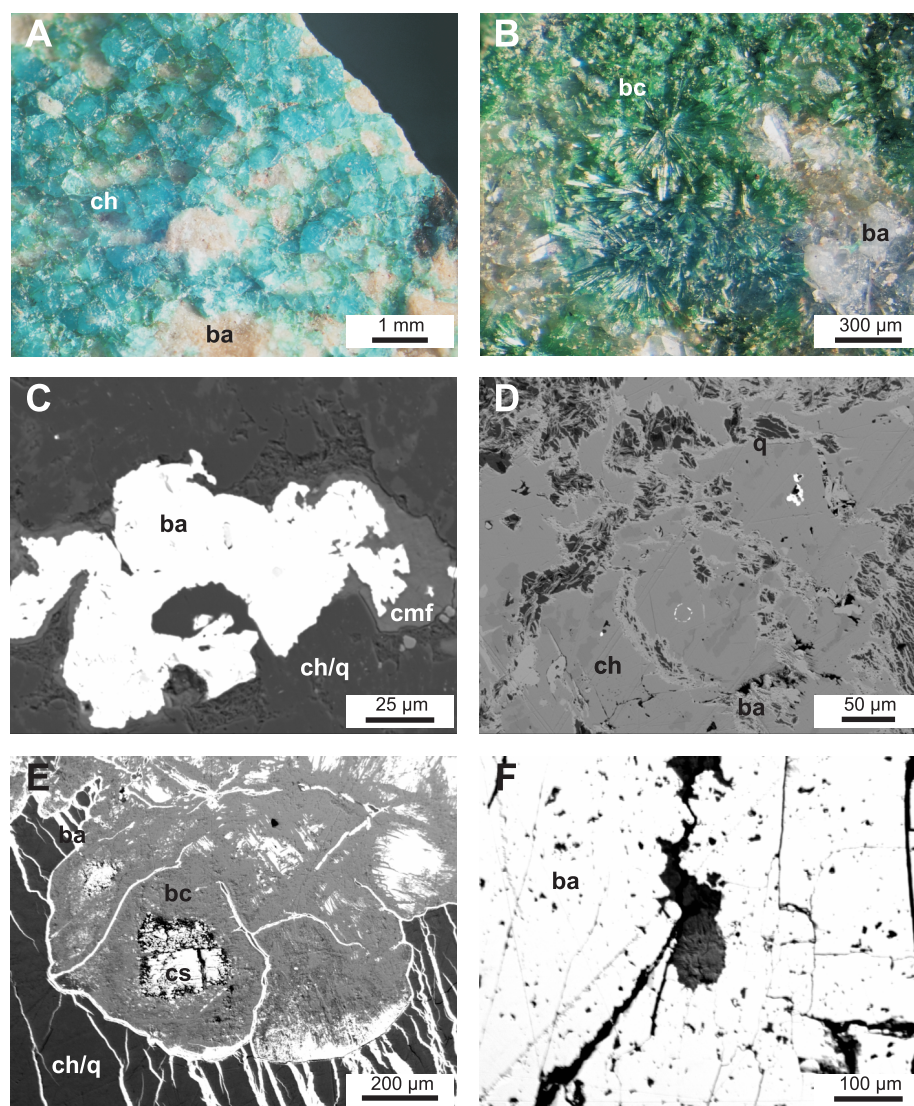


Fig. 5. Full-colour (A, B) and Back-Scattered-Electron (BSE, C–F) photomicrographs of the secondary assemblage from Stary Lesieniec

A – pseudomorphous bright blue chrysocolla (ch) in the baryte-rich matrix (ba); **B** – bright green sprays of brochantite (bc) needles among colourless baryte; **C** – BSE-bright baryte (ba) surrounded by chrysocolla/quartz (ch/q) and a Cu-Mg-Fe aluminosilicate (cmf); **D** – chrysocolla-dominated matrix with BSE-brighter veinlets of baryte and quartz, and tiny BSE-brightest inclusions of uraninite [and minor zircon and/or monazite-(Ce)]; **E** – large rounded aggregate of brochantite with inclusions of remnant Cu sulphides (cs), within chrysocolla/quartz matrix cut by baryte veinlets; **F** – tiny BSE-dark inclusion of either a Fe(Cu) aluminosilicate (in the middle) or hematite among chrysocolla

one sample; and $a = 13.153(7)\text{\AA}$, $b = 8.890(6)\text{\AA}$, $c = 5.987(3)\text{\AA}$, $\beta = 104.13(7)^\circ$ ($R_{wp} = 17.78\%$, GOF = 2.64%, DW = 0.32) for the second sample. Parameters obtained for malachite are: $a = 9.485(4)\text{\AA}$, $b = 11.955(4)\text{\AA}$, $c = 3.2443(9)\text{\AA}$, $\beta = 98.69(2)^\circ$ ($R_{wp} = 14.49\%$, GOF = 1.82%, DW = 0.63). The unit cell parameters of brochantite from the two samples studied are similar to each other, and variations are as low as 0.44 for a , 11 for b , 0.58 for c , and 1.2% for β . Larger discrepancies between the two calculated b parameters may be explained by a larger degree of freedom in the unit cell parameters variations due to the low (monoclinic) symmetry of brochantite. On the other hand, the quality of the second-sample refinement is lower and thus of

lower reliability. Typical published unit cell parameters of brochantite are $a = 13.08\text{\AA}$, $b = 9.85\text{\AA}$, $c = 6.02\text{\AA}$ and $\beta = 103.37^\circ$ (Anthony et al., 2003) and, thus, the difference is 0.12, 0.18, 0.03, and 0.44%, respectively, when compared with our data for the first sample. Due to the pure chemical nature of the brochantite studied (as explained below) the similarity of the values to these published ones are clear.

The secondary minerals studied are, in general, very pure chemically. The chemistry of chrysocolla is quite variable in terms of the proportions of its constituents, but not in terms of their chemical type.

Sample BK1. Examples of chrysocolla analyses are shown in Appendix 2 (analyses 1–5). SiO₂ varies in the 43.13–45.74 wt.% range and the corresponding ranges for Al₂O₃, CuO and CaO are 1.88–2.00, 45.73–46.90, and 0.87–1.10, respectively. The analyses recast to (Cu_{1.69}Al_{0.11}Ca_{0.05})_{Σ2.00}[H_{0.12}Si_{2.32}O₅](OH)_{3.50} · nH₂O (Cu + Al + Ca = 2 basis). Recasting these analyses to 4 atoms gives the formula (Cu_{1.71}Al_{0.11}Ca_{0.04})_{Σ1.85}[H_{0.11}Si_{2.15}O₅](OH)_{2.41} · nH₂O.

Some further Cu silicate species were detected in the sample BK1-1 (Appendix 3, analyses 1–7). These are disseminated in a quartz-rich matrix. The first species (phase A) is rich in Al and may be recasted to K_{0.97}(Mg_{1.52}Cu_{1.05}Fe_{0.21}Ca_{0.20}Ti_{0.01})_{Σ2.99}(Si_{9.05}Al_{5.88})_{Σ14.93}(O,OH)_{60.81} · n · mH₂O (*n* = 7, 18 cations basis, normalized by multiplication per 1.05). A single more silicic composition (phase B, Appendix 3, analysis 8) may be calculated to K_{1.02}(Mg_{1.42}Cu_{1.20}Ca_{0.22}Ti_{0.18})_{Σ3.02}(Al_{9.78}Fe_{0.30})_{Σ1.08}Si_{22.04}(O,OH)_{125.33} · n · mH₂O (36 cations basis). Yet another species (phase C, Appendix 3, analyses 9 and 10) may be expressed as (Cu_{1.70}Ca_{0.12}Mg_{0.03}K_{0.04}Fe_{0.01})_{Σ1.90}(Si_{4.42}Al_{0.11})_{Σ3.09}(O,OH)_{21.77} · n · mH₂O (16 cations basis).

Sample BK2. Examples of chrysocolla analyses are reported in Appendix 2 (analyses 6–11). The wt.% ranges are 40.47–48.20 for SiO₂, b.d.l. to 0.64 for Al₂O₃, 46.28–53.65 for CuO, and 0.22–0.46 for CaO. A single analysis shows 0.30 wt.% SO₃ and 0.22 wt.% P₂O₅ – possibly an interference. Recasted based on (Cu, Ca, Al) = 2 they give the empirical formula (*n* = 25) of (Cu_{1.97}Ca_{0.02}Al_{0.01})_{Σ2.00}(H_{0.01}Si_{2.41}O₅)(OH)_{3.66} · 0.74H₂O. Just a single analysis recasts to (Cu_{1.99}Ca_{0.02})_{Σ2.01}(Si_{1.99}S_{0.01}O₅)(OH)_{1.98} · nH₂O which corresponds to an “ideal” compound of the formula Cu₂(Si₂O₅)(OH)₂ · nH₂O (2 fewer hydroxyl groups being notable).

Brochantite composition (example analyses 1–10, Appendix 4), is Cu_{4.00}[(SO₄)_{1.08}(SiO₄)_{0.05}(PO₄)_{0.01}]_{Σ1.14}(OH)_{5.61} (*n* = 17). Its components vary in the following ranges (in wt.%): 0.19–0.79 SiO₂, 59.82–70.94 CuO, 15.92–17.71 SO₃, b.d.l. to 0.14 P₂O₅, and b.d.l. to 0.13 CaO. This relatively large variation is due both to different levels of sample destruction under the electron beam and the mineral habit (i.e., local porosity or thinning).

Also, the sample seems to bear yet another Cu silicate or a variety of chrysocolla. Initial analytical results (Appendix 3, analyses 11 and 12) suggest the first species, slightly depleted in both Si and Cu (phase D), may have its proposal formula of (Cu_{0.79}K_{0.14}Fe²⁺_{0.08}Ca_{0.02}Ti_{0.01})_{Σ1.04}(Al_{0.87}Fe³⁺_{0.09}P_{0.03})_{Σ0.99}Si_{1.92}[O_{5.67}(OH)_{1.33}]_{Σ7.00} · nH₂O (18 cations basis). The second one (phase E, Appendix 3, analyses 13–16) is possibly calculable to (K_{0.65}Ca_{0.09})_{Σ0.74}(Cu_{3.90}Mg_{0.34}Ti_{0.04})_{Σ5.09}(Fe_{0.81}Al_{0.19})_{Σ1.00}(Si_{8.37}Al_{3.51}P_{0.09}S_{0.04})_{Σ12.01}O_{28.04}[(OH)_{0.96}Cl_{0.05}]_{Σ1.01} · nH₂O (*n* = 5, same basis). As compared to other minerals studied, both the phases D and E are Fe- and Ti-enriched, with maximum contents of up to 4.22 wt.% FeO and 0.28 wt.% TiO₂. They are also characterized by slight P (up to 0.49 wt.% P₂O₅) and Cl (up to 0.15 wt.%) enrichment. Besides, phase E is enriched in S (up to 0.10 wt.% SO₃). Of all the phases A–E, the highest amounts of K and Mg are found in phase A (up to 4.43 wt.% K₂O and 7.37 wt.% MgO). The rather stable level of Cl enrichment excludes epoxy resin interference.

Sample BK3-1. Control samples of a chrysocolla-like material (Appendix 2, analyses 12–14) show, on average, 47.81 wt.% SiO₂, 3.69 wt.%, Al₂O₃, 39.12 wt.% CuO, 1.43 wt.% CaO, 0.16 wt.% MgO, 0.12 wt.% K₂O, and 0.06 wt.% Cl. This chrysocolla is thus different from the above examples due to

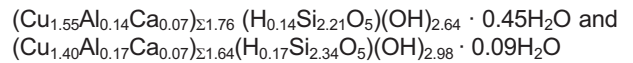
slight enrichment in K, Mg, and Cl. The analyses recast to (Cu_{1.65}Al_{0.24}Ca_{0.09}Mg_{0.01}K_{0.01})_{Σ2.00}(H_{0.24}Si_{2.67}O₅)(OH) · nH₂O (Cu + Al + Ca + Mg + K = 2 basis).

The brochantite composition (*n* = 17, with example analyses 10–16 in Appendix 4) is Cu_{3.97}[(SO₄)_{0.98}(SiO₄)_{0.03}]_{Σ1.02}(OH)_{5.86}. This brochantite is slightly more pure than the above-described one. Variations of its components, in wt.%, are: b.d.l. to 1.17 SiO₂, 70.47–74.90 wt.% CuO, 16.98–18.20 SO₃, and b.d.l. to 0.19 CaO.

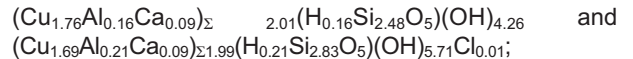
The brochantite is associated with a slightly P-enriched phase that also bears trace Si and S. It is most likely malachite (Appendix 5), especially that CO₃-PO₄-SO₄-SiO₄ substitution is known in minerals (e.g., in the apatite supergroup; e.g., Kruszewski, 2008). Its composition is (*n* = 10) Cu_{2.00}[(CO₃)_{0.92}(SO₄)_{0.05}(PO₄)_{0.01}(SiO₄)_{0.01}]_{Σ0.99}(OH)_{2.00}. Variation of its components is as follows (in wt.%): b.d.l. to 0.52 SiO₂, 67.28–68.26 CuO, b.d.l. to 3.81 SO₃, and 0.17–0.53 P₂O₅.

Sample BK3-2. Two varieties of a Cu-Si-O(H) phase were detected, with representative analyses in Appendix 2 numbered 15–17 (type 1) and 18–20 (type 2). The observed variation of their constituents, in wt.%, is 41.47–48.37 SiO₂, 1.56–3.41 Al₂O₃, 35.85–47.08 CuO, and 1.02–1.43 CaO. A single analysis shows 0.02 wt.% ZnO and 0.50 wt.% K₂O. As much as 2 in 13 analyses show a small P admixture. Recasting (*n* = 12 and *n* = 3, respectively) gives the following results:

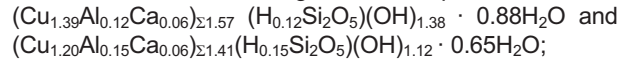
- based on 4 total cations (including Si), to give the empirical formulae:



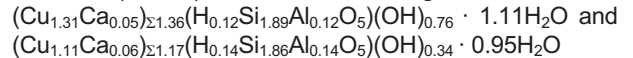
- based on (Cu + Al + Ca) = 2, with the following empirical formulae:



- based 2 Si atoms, to give the empirical formulae:



- based on (Si + Al) = 2, with the following related formulae:



Neither of these formulae fit the supposed ideal chrysocolla constitution. Normalizing the wt.% results with the use of (Cu,Al,Ca) oxides/SiO₂ ratios does not pose a large difference to the above formulae thus providing a likely confirmation that at least the chrysocolla studied is not a single compound with precisely attributable ideal composition.

Two supposed chrysocolla analyses recast to gilalite, (Cu_{4.81}Ca_{0.14})_{Σ4.95}(Si_{5.76}Al_{0.27}P_{0.02})_{Σ5.90}[O_{16.92}Cl_{0.02}]_{Σ16.94} · 4.83H₂O (ideally Cu₅Si₆O₁₇ · 7H₂O; lower water content possibly due to dehydration), but this species was not confirmed via PXRD. Another minor phase observed in the sample is a supposed Fe-dominant Cu-bearing aluminosilicate (Fig. 5F) with the following wt.% ranges: SiO₂ 8.14–8.75, TiO₂ 0.48–0.49, Fe₂O₃ 76.73–77.77, Al₂O₃ 1.12–1.26, CuO 5.04–6.02, CaO 0.31–0.39, MgO up to 0.17, Cl up to 0.06, and K, Mn, Zn, S, P, As, and V below their detection limits. With totals >92% the phase can be recasted, e.g., to (Fe³⁺_{6.35}Cu_{0.46}Ti_{0.04}Ca_{0.04}Mg_{0.02})_{Σ6.91}(Si_{0.94}Al_{0.05})_{Σ0.99}O_{12.06} · 2.45H₂O (*n* = 3). However, tiny hematite crystals are also found within voids in chrysocolla and the above analyses may simply be erroneous due to possible mixed-information character.

DISCUSSION

PARAGENETIC SEQUENCE OF THE EPITHERMAL MINERALIZATION AT STARY LESIENIEC

At most locations known from the literature copper sulphide paragenesis coexists with chalcopyrite and bornite, which crystallize at the first stages and then – with decreasing temperature – transform into simple sulphides of the Cu-S system (e.g., Hatert, 2005). In the hydrothermal system at Stary Lesieniec undersaturated in iron, chalcopyrite and bornite are absent. The same is true for pyrite which is otherwise common in hydrothermal systems. Most simple copper sulphides, such as chalcocite, occur in cementation zones within supergene enrichment parts of various copper deposits (e.g., Belogub et al., 2008; Vlasáč et al., 2018). At Stary Lesieniec, copper sulphides are related to primary, epithermal mineralization.

Formation stages and the paragenetic sequence of Cu mineralization at Stary Lesieniec are shown in Figure 6. At the hydrothermal stage at the site studied crystallization began with idiomorphic quartz. Then, the main chalcocite masses were formed. Within the aggregates of chalcocite, uraninite also appeared. Uraninite inclusions have also been found in the chrysocolla, which may indicate that it crystallized within the limits of the epithermal stage. According to Pohjola (2015), the UO_2^{2+} (uranyl) ions dissolved in hydrothermal fluids running along faults may be deposited as uraninite in contact with country rocks. Younger than the chalcocite is djurleite, which formed irregular zones and intergrowths with chalcocite.

The next stage is anilite/digenite formation with the minerals deposited as elongated lamellae along the cleavage planes of chalcocite and djurleite. The copper-mineralized zones were then filled with idiomorphic baryte crystals, which are known

from many locations within the Intra-Sudetic Basin and Sowie Mts. (e.g., Kruszewski et al., 2019; Pršek et al., 2019; Mederski et al., 2020). Baryte crystals are characterized by the presence of numerous hematite inclusions. Hydrothermal hematite is known (e.g., Dalstra and Guedes, 2004) and many papers describe the hydrothermal synthesis of this species (e.g., Tadic et al., 2019). Sun et al. (2015), who characterized some BIF-type iron deposits, mentioned a few habit varieties of hematite, with a needle-like to fibrous one being a late-stage replacement related to fluid activity. We thus suggest the Stary Lesieniec hematite is related to the hydrothermal activity. Chrysocolla in the studied copper-baryte mineralization crystallized both at the epithermal and supergene stages; the interpretation of the conditions of its formation is described below.

Uranium hydrothermal occurrences within the Intra-Sudetic Basin are known from the secondary hematitization zones of rhyolites (e.g., Plewa, 1965; Migaszewski, 1972). Migaszewski (1972) described pitchblende growing around pyrite crystals in porphyry from the Boguszów baryte deposit. Moreover, similar mineralization was described from a borehole within the secondary hematitization zone of the Upper Carboniferous Chelmiec rhyolite laccolith. There, uraninite is in paragenesis with hematite, galena, and pyrite (Migaszewski, 1972). In addition, uranium mineralization is known from the Mieszko Coal Mine in Wałbrzych, where pitchblende occurs in the contact zones of coal seams with the porphyry body, or in veins of dark grey and cherry-red dolomite (Plewa, 1965). Pitchblende is there associated with dolomite, siderite, marcasite, pyrite, and secondary uranium and copper minerals. Sylwestrzak (1972) pointed out that the average uranium content of the Carboniferous porphyries (5.49 ppm) is significantly higher than that in the Permian volcanic rocks (3.18 ppm) and is not related to the mineralogical composition of the rock. This indicates secondary hydrothermal enrichment in uranium of these volcanic rocks. Moreover, U enrichment in the Žácleř and Glinik formations within the Intra-Sudetic Basin is related to epigenetic activity (Miecznik, 1989).

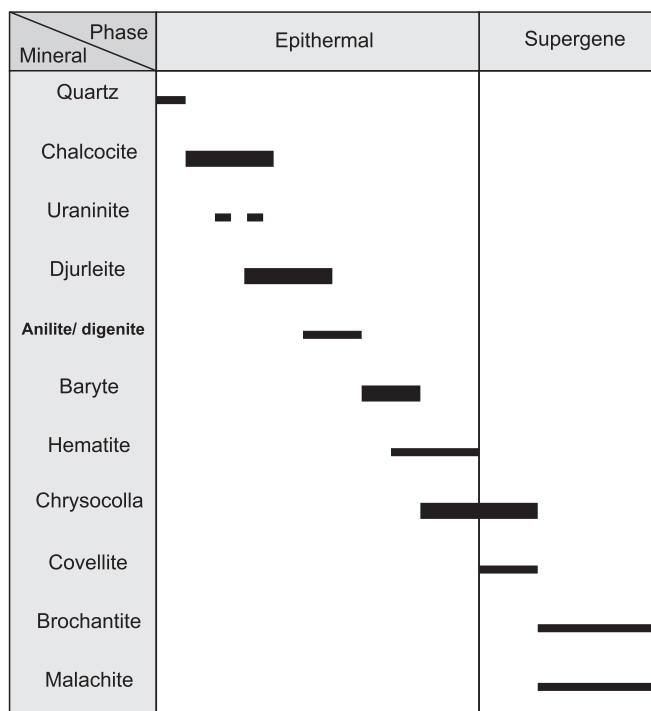


Fig. 6. Formation stages and the paragenetic sequence of Cu mineralization in the Stary Lesieniec rhyolite quarry

CRYSTALLIZATION TEMPERATURES OF THE EPITHERMAL PARAGENESIS AT STARY LESIENIEC

PXRD studies confirmed the presence of monoclinic low-chalcocite and the absence of hexagonal high-chalcocite in the system studied. According to Evans (1981), the transition temperature for these two polymorphs of chalcocite is 103.5°C (Fig. 7). Therefore, the initial temperature of the crystallization of copper sulphides did not exceed 103.5°C. The presence of younger djurleite forming irregular zones and replacing chalcocite indicates a decrease in the crystallization temperature, the upper limit of stability of djurleite being 93°C (Fig. 7) (Evans, 1981). The youngest Cu sulphide in the epithermal stage of the paragenetic sequence at Stary Lesieniec was anilite/digenite. The interpretation of PXRD analyses tends to lead to anilite over digenite, even though the chemistry tends to be digenite. A mismatch of the obtained chemical formula of anilite/digenite and the PXRD results is probably due to the transformation of anilite into a phase similar to digenite, as a result of sample polishing and drying (Morimoto et al., 1969; Morimoto and Koto, 1970). Anilite is stable <70 ±3°C (Fig. 7) and, as a result of heating, it is decomposed and transformed to high digenite and covellite (Morimoto et al., 1969; Morimoto and Koto, 1970). The anilite described by us crystallized in the conditions of the stability field for anilite and djurleite (Fig. 7). On the other hand, covellite crystallized at the following, supergene stage (Fig. 7). In conclusion, the copper sulphide studied from

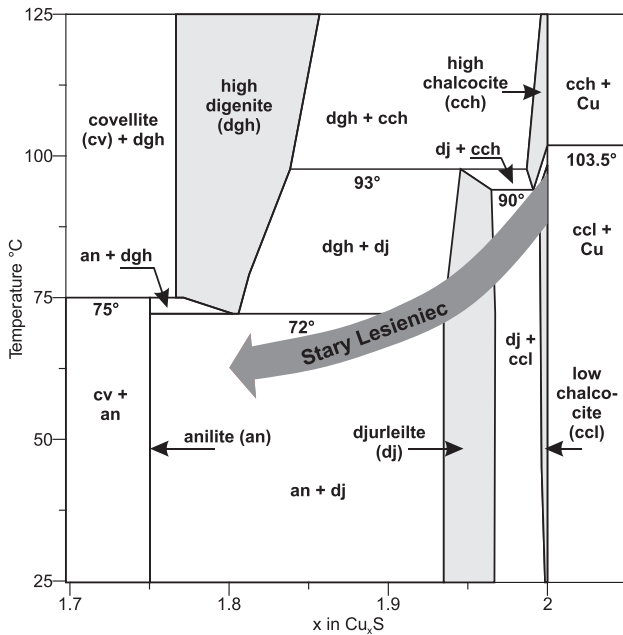


Fig. 7. Phase diagram for the Cu-S system in the low-temperature region near Cu_2S composition; adapted from Potter (1977) and Evans (1981)

Stary Lesieniec began crystallization at temperatures of $\sim 100^\circ\text{C}$, and then during the epithermal stage of precipitation, the temperature of the solutions cooled to $<72^\circ\text{C}$ (Fig. 7).

The presence of uraninite is interpreted as to its belonging to the epithermal stage. Uraninite crystallization is usually reported to take place at $>200^\circ\text{C}$ (e.g., Eriksson et al., 2004). According to Yuan et al. (2019), at $100\text{--}400^\circ\text{C}$, uraninite (hydrothermally deposited at $250\text{--}450^\circ\text{C}$) dissolves and becomes a precursor for the U^{4+} silicate mineral coffinite. The formation of uraninite at low temperatures is favoured by acidic conditions (Cui et al., 2015). Additionally, Rojkovič et al. (1993) described formation temperatures of Cu-U mineralization from Novoveská Huta in Slovakia ranging from 95 to 190°C . These temperatures were determined for the younger Cu-U mineralized veins that intersect older stratiform deposits and host copper mineralization with uraninite and coffinite. The lower temperature range for the Novoveská Huta mineralization may correspond to the temperature ranges of chalcocite formation at Stary Lesieniec. The local uraninite crystallization either (1) preceded that of chalcocite, with possible co-deposition, or (2) took place after the dissolution of some earlier inclusions. Indeed, some marks of possible inclusion dissolution were observed in the material studied. If the latter is true, then the Ca, Mn-dominant diadochy in the uraninite suggests such primary inclusions to be some carbonate minerals which are well known for being a Ca, Mn-sink.

SECONDARY Cu MINERAL PARAGENESIS AND ITS FORMATION CONDITIONS

Chrysocolla is the most common secondary mineral in the copper-baryte mineralization studied from Stary Lesieniec. Farges et al. (2007) redefined chrysocolla as a "mesoscopic assemblage composed dominantly as spertiniite $[\text{Cu}(\text{OH})_2]$, water and amorphous silica (SiO_2)". However, other authors do not support such findings. They, e.g., state that chrysocolla is rather a copper silicate colloidal gel (Frost and Xi, 2013), or an

amorphous Cu silicate with some structural aspects related to those of tenorite and diopside, but not Cu^0 or cuprite (McKeown, 1994). The experimental studies of Hariu et al. (2013) also suggest the compound to be a Cu silicate gel, with variable Cu/Si mole ratios, with PXRD image precluding single-crystal study for determination of the structural model. Although Frost et al. (2012) seemed to confirm chrysocolla as a separate mineral species, they reported false-correct (i.e., close to the "ideal" composition) empirical formulae as these are based on standardless EDX analyses with 100% total normalization. As such, the first author's theory is not necessarily completely wrong: various chrysocollas may exist. This would explain the large discrepancies between the proposed empirical formulae and the supposed ideal formula of chrysocolla. Nevertheless, studying its composition (in particular, the Cu content) is reasonable due to the proposed usage of this compound as a Cu ore (e.g., Gijsemans et al., 2020). The Cu (alumo)silicate species with representative analyses listed in Appendix 2 may be some new species, or varieties, of chrysocolla. We are aware of the further analyses needed to be performed for either approval or disapproval of such proposal stoichiometry and site representations.

The chrysocolla-bearing paragenesis at Radzimowice, Lower Silesia, occurs as thin encrustations in rhyolite's cracks (Siuda and Kruszewski, 2013). The authors suggested the rhyolite, and surrounding rocks, as a source of silica. At Stary Lesieniec silica must have been derived from the rock-matrix aluminosilicates contacting with acidic solutions formed due to oxidation of the ore. Chrysocolla could have been formed via interaction of such post-oxidation solutions, released silica, and meteoric waters allowing for pH increase (e.g., Schlomovitch et al., 1999). As the first secondary weathering copper mineral, chrysocolla recorded pH values most likely close to neutral ones (e.g., Crane et al., 2001).

According to Frost et al. (2012), chrysocolla begins to thermally decompose at $\sim 125^\circ\text{C}$. Thus, it should still be stable at the moderate/low-temperature hydrothermal stage of mineralization. The upper-temperature limit given for the Cu sulphides (103.5°C) is close to the one marking the thermal stability of chrysocolla. The upper pH limit of the whole secondary assemblage is supported by the complete inertness of chrysocolla to leaching at the pH of 6. Also, the mineral is easily leached at $\text{pH} < 3$ (Nikol and Akilan, 2018). On the other hand, Herrera-Urbina et al. (2010), who addressed the known published issue of chrysocolla flotation, suggested the removal of significant amounts of Cu from the mineral already at $\text{pH} < 6$. Thus, the local chrysocolla stability may have been in the narrow 6–7 pH range. A following drop in pH allowed for the release of Cu, most likely from both chrysocolla and some sulphides, and led to precipitation of brochantite. Brochantite is the most stable hydrous copper sulphate mineral (e.g., Marani et al., 1995), with a relatively wide stability range of $\text{pH} = 4\text{--}7.5$ (Bridges and Green, 2007). However, the absence of langite and posnjakite suggests an upper pH limit of ~ 6 (Alwan and Williams, 1979). The mineralizing solutions of the supergene weathering stage must have been occasionally enriched in CO_3^{2-} ions, as reflected by the rare occurrence of malachite.

CONCLUSIONS

1. Examples of copper-baryte mineralized veinlets were found covering the western walls of the Stary Lesieniec rhyolite quarry.

2. A general succession of crystallization for the epithermal stage is as follows: quartz–chalcocite–djurleite–anilite/digenite–baryte–hematite–chrysocolla; the supergene stage is represented by: chrysocolla + covellite, followed by brochantite + malachite.

3. The copper sulphides studied began to crystallize at temperatures of ~100°C; then, during the epithermal stage of precipitation, the temperature of the solutions dropped to <72°C.

4. The supergene oxidation processes began with the formation of abundant chrysocolla, at a relatively neutral pH. Following a pH drop, to ~4–6, brochantite was deposited. The mineralizing solutions were only rarely enriched in carbonate anions, as reflected by the rare occurrence of malachite.

Acknowledgements. We are grateful to A. Włodek from the Laboratory of Critical Elements at AGH-UST and B. Marciński-Maliszewska from the Inter-Institution Laboratory of Microanalysis of Minerals and Synthetic Substances UW for help during EPMA data collection. We are also grateful to the anonymous reviewers, whose comments helped us to improve the manuscript. Also, the authors would like to thank K. Pytel - who discovered the Cu mineralization studied – for sharing this find with us. This work is part of the research program financed by the AGH University of Science and Technology statutory grant No. 11.11.140.320 and 2020 statutory funding of the Ministry of Higher Education and Science for the IGS PAS.

REFERENCES

- Alwan, A.K., Williams, P.A., 1979.** Mineral formation from aqueous solution. Part II. The stability of langite, $\text{Cu}_2\text{SO}_4(\text{OH})_6\text{H}_2\text{O}$. *Transition Metal Chemistry*, **4**: 319–322.
- Anthony, J.W., Bideaux, R.A., Bladh, K.W., Nichols, M.C., 2003.** *Handbook of Mineralogy*, 5. Borates, Carbonates, Sulfates. Mineral Data Publishing, Tucson.
- Awdankiewicz, M., 1998.** Volcanism in a late Variscan intramontane trough: Carboniferous and Permian volcanic centres of the Intra-Sudetic Basin, SW Poland. *Geologia Sudetica*, **32**: 13–47.
- Awdankiewicz, M., 1999.** Volcanism in a late Variscan intramontane trough: the petrology and geochemistry of the Carboniferous and Permian volcanic rocks of the Intra-Sudetic Basin, SW Poland. *Geologia Sudetica*, **32**: 83–111.
- Awdankiewicz, M., Kurowski, L., Mastalerz, K., Raczyński, P., 2003.** The Intra-Sudetic Basin – a record of sedimentary and volcanic processes in late- to post-orogenic tectonic setting. *Geolines*, **16**: 165–183.
- Belogub, E.V., Novoselov, K.A., Yakovleva, V.A., Spiro, B., 2008.** Supergene sulphides and related minerals in the supergene profiles of VHMS deposits from the South Urals. *Ore Geology Reviews*, **33**: 239–254.
- Bridges, T.T., Green, D.J., 2007.** Zoned oxidation deposit in Tynebottom Mine, Garrigill, Cumbria. *Journal of the Russell Society*, **10**: 2–9.
- Cabral, A.R., Beaudoin, G., 2007.** Volcanic red-bed copper mineralisation related to submarine basalt alteration, Mont Alexandre, Quebec Appalachians, Canada. *Mineralium Deposita*, **42**: 901–912.
- Cook, W.R., 1972.** Phase changes in Cu_2S as a function of temperature. *National Bureau of Standards Publication*, **364**: 703–712.
- Crane, M.J., Sharpe, J.L., Williams, P.A., 2001.** Formation of chrysocolla and secondary copper phosphates in the highly weathered supergene zones of some Australian deposits. *Records-Australian Museum*, **53**: 49–56.
- Cui, C.L., Li, Q., Zhang, D., Wang, X.L., Wu, T., Zhang, L., Yi, F.C., 2015.** Formation conditions of uraninite and mineralogical analysis in uranium-containing waste water. *Journal of Chengdu University of Technology*, **1**: 122–128.
- Dalstra, H., Guedes, S., 2004.** Giant hydrothermal hematite deposits with Mg-Fe metasomatism: a comparison of the Carajás, Hamersley, and other iron ores. *Economic Geology*, **99**: 1793–1800.
- Dumańska-Słowik, M., Natkaniec-Nowak, L., Kotarba, M.J., Sikorska, M., Rzymelka, J.A., Łoboda, A., Gawel, A., 2008.** Mineralogical and geochemical characterization of the “bituminous” agates from Nowy Kościół (Lower Silesia, Poland). *Neues Jahrbuch für Mineralogie*, **184**: 255–268.
- Emetz, A., Piestrzyński, A., Zagnitko, V., Pryhodko, L., Gawel, A., 2006.** Geology, mineralogy and origin of Zhyrychi native copper deposit (North-Western Ukraine). *Annales Societatis Geologorum Poloniae*, **76**: 297–314.
- Eriksson, P.G., Altermann, W., Nelson, D.R., Mueller, W.U., Catuneanu, O., 2004.** Evolution of the Hydrosphere and Atmosphere. *Developments in Precambrian Geology*, **12**: 359–511.
- Estep, C., 2012.** *Compounds of Uranium and Fluorine (Chemical Compounds)*. Research World, Delhi, India.
- Evans, H.T., 1981.** Copper coordination in low chalcocite and djurleite and other copper-rich sulfides. *American Mineralogist*, **66**: 807–818.
- Farges, F., Benzerara, K., Brown, G.E. Jr., 2007.** Chrysocolla Re-defined as Spertiniite. 13th International Conference On X-Ray Absorption Fine Structure (XAFS13), July 9–14, Stanford, California, SLAC-PUB-12332. doi: 10.1063/1.2644481
- Ferenc, Š., Rojkovič, I., 2001.** Copper mineralization in the Permian basalts of the Hronicum unit, Slovakia. *Geolines*, **13**: 22–27.
- Frost, R.L., Xi, Y., 2013.** Is chrysocolla $(\text{Cu},\text{Al})_2\text{H}_2\text{Si}_2\text{O}_6(\text{OH})_4 \cdot n\text{H}_2\text{O}$ related to spertiniite $\text{Cu}(\text{OH})_2$? – a vibrational spectroscopic study. *Vibrational Spectroscopy*, **64**: 33–38.
- Frost, R.L., Xi, Y., Wood, B.J., 2012.** Thermogravimetric analysis, PXRD, EDS and XPS study of chrysocolla $(\text{Cu},\text{Al})_2\text{H}_2\text{Si}_2\text{O}_5(\text{OH})_4 \cdot n\text{H}_2\text{O}$ – structural implications. *Thermochemica Acta*, **545**: 157–162.
- Gablina, I.F., Semkova, T.A., Stepanova, T.V., Gor'kova, N.V., 2006.** Diagenetic alterations of copper sulfides in modern ore-bearing sediments of the Logatchev-1 hydrothermal field (Mid-Atlantic Ridge 14 45' N). *Lithology and Mineral Resources*, **41**: 27–44.
- Gijsemans, L., Roosen, J., Riaño, S., Jones, P.T., Binnemans, K., 2020.** Ammoniacal solvleaching of copper from high-grade chrysocolla. *Journal of Sustainable Metallurgy*, **6**: 589–598.
- Goble, R.J., 1980.** Copper sulphides from Alberta: yarrowite Cu_9S_8 and spionkopite $\text{Cu}_{39}\text{S}_{28}$. *Canadian Mineralogist*, **18**: 511–518.
- Goble, R.J., 1981.** The leaching of copper from anilite and production of a metastable copper sulfide structure. *Canadian Mineralogist*, **19**: 583–591.
- Goble, R.J., Robinson, G., 1981.** Geerite $\text{Cu}_{1.6}\text{S}$, a new copper sulfide from Dekalb township, New York. *Canadian Mineralogist*, **18**: 519–523.
- Gołębiowska, B., Matyszkiewicz, J., Molenda, R., Górný, A., 2006.** Hydrothermal mineralization in Middle Jurassic sandy limestones from Zalas (near Cracow, S Poland). *Mineralogia Polonica, Special Papers*, **28**: 81–83.
- Grocholski, A., 1965.** The volcanic rocks in the Walbrzych Basin in the light of structural studies (in Polish with English summary). *Biuletyn Instytutu Geologicznego*, **191**: 5–67.
- Grocholski, A., 1973.** Szczegółowa mapa geologiczna Sudetów 1:25 000, arkusz Mieroszów (in Polish). *Wyd. Geol., Warszawa*.

- Hariu, T., Arima, H., Sugiyama, K., 2013.** The structure of hydrated copper-silicate gels, an analogue compound for natural chrysocolla. *Journal of Mineralogical and Petrological Sciences*, **108**: 111–115.
- Hatert, F., 2005.** Transformation sequences of copper sulfides at Vielsalm, Stavelot Massif, Belgium. *Canadian Mineralogist*, **43**: 623–635.
- Herrera-Urbina, H., Laskowski, J.S., Fuerstenau, D., 2010.** A proces for the flotation of chrysocolla. XXV International mineral processing congress – IMP 2010. Congress Proceedings, Australasian Institute of Mining and Metallurgy, Brisbane: 1959–1969.
- Holub, V.M., 1976.** Permian basins in the Bohemian Massif. In: *The Continental Permian in Central, West, and South Europe* (ed. H. Falke): 53–79. Dordrecht.
- Kettanah, Y.A., 2019.** Copper mineralization and alterations in Gercus Basalt within the Gercus Formation, northern Iraq. *Ore Geology Reviews*, **111**: 102974.
- Konari, M.B., Rastad, E., Kojima, S., Omran, N.R., 2013.** Volcanic redbed-type copper mineralization in the Lower Cretaceous volcano-sedimentary sequence of the Keshtmahaki deposit, southern Sanandaj-Sirjan Zone, Iran. *Neues Jahrbuch für Mineralogie-Abhandlungen*, **190**: 107–121.
- Kozłowski, S., 1958.** Permian volcanism in the area of Głuszyca and Świerki (Lower Silesia, Poland) (in Polish with English summary). *Annales Societatis Geologorum Poloniae*, **28**: 5–61.
- Kozłowski, S., 1963.** The geology of Permian volcanites in the central part of the inner Sudetic depression (Lower Silesia) (in Polish with English summary). *Prace Geologiczne*, **14**: 3–84.
- Krawczyński, W., 1995.** Native copper in agates from Rudno near Krzeszowice. *Mineralogia Polonica*, **26**: 27–32.
- Kruszewski, Ł., 2008.** Apatite-ellestadite solid solution and associated minerals of metacarbonate slags from burning coal dump in Rydułtowy (Upper Silesia). *Mineralogia Special Papers*, **32**: 100.
- Kruszewski, Ł., 2013.** Supergene sulphate minerals from the burning coal mining dumps in the Upper Silesian Coal Basin, South Poland. *International Journal of Coal Geology*, **105**: 91–109.
- Kruszewski, Ł., Siuda, R., Kosalka, P., Żochowski, P., Marciniak-Maliszewska, B., Deput, E., 2019.** Copper and manganese minerals from „Hans” mine in Przygórze (Lower Silesia, SW Poland) – preliminary results. *Mineralogia Special Papers*, **49**: 56.
- Large, D.J., MacQuaker, J., Vaughan, D.J., Sawłowicz, Z., Gize, A.P., 1995.** Evidence for low-temperature alteration of sulfides in the Kupferschiefer copper deposits of southwestern Poland. *Economic Geology*, **90**: 2143–2155.
- Lorenz, V., Nicholls, I.A., 1976.** The Permo-carboniferous basin and range province of Europe. An application of plate tectonics. In: *The Continental Permian in Central, West and South Europe* (ed. H. Falke): 313–342. Springer International Publishing, Dordrecht.
- Marani, D., Patterson, J.W., Anderson, P.R., 1995.** Alkaline precipitation and aging of Cu(II) in the presence of sulfate. *Water Research*, **29**: 1317–1326.
- Mathur, R., Falck, H., Belogub, E., Milton, J., Wilson, M., Rose, A., Powell, W., 2018.** Origins of chalcocite defined by copper isotope values. *Geofluids*, **2018**; doi: 10.1155/2018/5854829
- McKeown, D.A., 1994.** X-ray absorption spectroscopic study of copper in an amorphous copper silicate: chrysocolla. *Journal of Non-crystalline Solids*, **180**: 1–10.
- Mederski, S., Pršek, J., Niemasz, Ż., 2020.** Geochemistry of tetrahedrite group minerals and associated silver paragenesis in the Boguszów baryte deposit, Poland. *Geological Quarterly*, **64** (4): 958–968.
- Miecznik, J.B., 1989.** Uranium mineralization in the Permo-Carboniferous of the Intra-Sudetic Depression (in Polish with English summary). *Przegląd Geologiczny*, **37**: 485–488.
- Migaszewski, Z., 1972.** Mineralizacja kruszczowa w złożu barytu w Boguszowice (in Polish). *Rudy i Metale Nieżelazne*, **9**: 425–428.
- Mikulski, S., 2005.** Geological, mineralogical and geochemical characteristics of the Radzimowice Au-As-Cu deposit from the Kaczawa Mts. (Western Sudetes, Poland) – an example of the transition of porphyry and epithermal style. *Mineralium Deposita*, **39**: 904–920.
- Mikulski, S.Z., Williams, I.S., 2014.** Zircon U-Pb dating of igneous rocks in the Radzimowice and Wielisław Złotoryjski auriferous polymetallic deposits, Sudetes, SW Poland. *Annales Societatis Geologorum Poloniae*, **84**: 213–233.
- Mikulski, S.Z., Oszczepalski, S., Sadłowska, K., Chmielewski, A., Malek, R., 2020.** Trace element distributions in the Zn-Pb (Mississippi Valley-type) and Cu-Ag (Kupferschiefer) sediment-hosted deposits in Poland. *Minerals*, **10**, 75.
- Mochacka, K., Oberc-Dziedzic, T., Mayer, W., Pieczka, A., 2012.** Ore mineralization in the Miedzianka area (Karkonosze-Izera Massif, the Sudetes, Poland): new information. *Mineralogia*, **43**: 155–178.
- Morimoto, N., Koto, K., 1970.** Phase relations of the Cu-S system at low temperatures: stability of anilite. *American Mineralogist*, **55**: 106–117.
- Morimoto, N., Koto, K., Shimazaki, Y., 1969.** Anilite, Cu₇S₄, a new mineral. *American Mineralogist: Journal of Earth and Planetary Materials*, **54**: 1256–1268.
- Nemec, W., 1979.** Wulkanizm późnkarboński w niecce wałbrzyjskiej (synklinorium śródsudeckie) (in Polish). PhD Thesis, Uniwersytet Wrocławski, Wrocław.
- Németh, N., Földessy, J., Turi, J., 2017.** Ore geology of the copper sulfide mineralization in the Rudabánya ore-bearing complex. *Central European Geology*, **60**: 53–72.
- Nikol, M.J., Akilan, C., 2018.** The kinetics of the dissolution of chrysocolla in acid solutions. *Hydrometallurgy*, **178**: 7–11.
- Palyanova, G., Sidorov, E., Borovikov, A., Seryotkin, Y., 2020.** Copper-containing agates of the Avacha Bay (Eastern Kamchatka, Russia). *Minerals*, **10**, 1124.
- Parafiniuk, J., Siuda, R., Borkowski, A., 2016.** Sulphate and arsenate minerals as environmental indicators in the weathering zones of selected ore deposits, Western Sudetes, Poland. *Acta Geologica Polonica*, **66**: 493–508.
- Pawley, G.S., 1980.** EDINP, the Edinburgh powder profile refinement program. *Journal of Applied Crystallography*, **13**: 630–633.
- Pieczonka, J., Piestrzyński, A., Lenik, P., Czerw, H., 2007.** Distribution of ore minerals in the copper deposit, Fore-Sudetic Monocline, SW Poland. *Biuletyn Państwowego Instytutu Geologicznego*, **423**: 95–108.
- Piestrzyński, A., Kowalik, K., 2015.** Argentopentlandite from baryte vein in Zagórze Śląskie, Lower Silesia, a first occurrence in Poland. *Mineralogia*, **45**: 13–25.
- Plewa, M., 1965.** Hematyzacja intruzywnych skał „porfirowych” i towarzyszących im dolomitów, występujących w kopalni Mieszko w Wałbrzychu (in Polish). *Sprawozdania z Posiedzeń Komisji PAN Oddziału w Krakowie*, **8**: 502–505.
- Pohjolainen, E., 2015.** Uranium deposits of Finland. In: *Mineral Deposits of Finland* (eds. W.D. Maier, R. Lahtinen and H. O'Brien). Elsevier.
- Potter, R.W., 1977.** An electrochemical investigation of the system copper-sulfur. *Economic Geology*, **72**: 1524–1542.
- Powolny, T., Dumańska-Słowik, M., Sikorska-Jaworowska, M., Wójcik-Bania, M., 2019.** Agate mineralization in spilitized Permian volcanics from “Borówno” quarry (Lower Silesia, Poland) – microtextural, mineralogical, and geochemical constraints. *Ore Geology Reviews*, **114**: 103130.
- Pósfai, M., Buseck, P.R., 1994.** Djurleite, digenite, and chalcocite: Intergrowths and transformations. *American Mineralogist*, **79**: 308–315.
- Pršek, J., Mederski, S., Kowalczyk, D., 2019.** Ag-Sb-Pb-Cd mineral paragenesis in the baryte veins: example from the Sowie Mountains, Poland. *Life with Ore Deposits on Earth. 15th Biennial SGA Meeting, 27–30 August 2019, Glasgow*, **1**: 455–458.
- Rietveld, H.M., 1967.** Line profiles of neutron powder-diffraction peaks for structure refinement. *Acta Crystallographica*, **22**: 151–152.
- Rojkovič, I., 1990.** Ore bearing Permian volcanism in the Western Carpathians. *Acta Geologica et Geographica Universitatis Comenianae. Geologica*, **45**: 71–88.

- Rojkovič, I., Novotny, L., Háber, M., 1993.** Stratiform and vein U, Mo and Cu mineralization in the Novoveská Huta area, CSFR. *Mineralium Deposita*, **28**: 58–65.
- Roseboom, E.H., 1966.** An investigation of the system Cu-S and some natural copper sulfides between 25° and 700°C. *Economic Geology*, **61**: 641–672.
- Sawłowicz, Z., 1990.** Primary copper sulphides from the Kupferschiefer, Poland. *Mineralium Deposita*, **25**: 262–271.
- Schlomovitch, N., Bar-Matthews, M., Segev, A., Matthews, A., 1999.** Sedimentary and epigenetic copper mineral assemblages in the Cambrian Timna Formation, southern Israel. *Israel Journal of Earth Sciences*, **48**: 195–208.
- Schmidt, J.A., Sagua, A.E., Lescano, G., 1998.** Electrochemical investigation of the equilibria (covellite + anilite) and (covellite + digenite). *The Journal of Chemical Thermodynamics*, **30**: 283–290.
- Sillitoe, R.H., Clark, A.H., 1969.** Copper and copper-iron sulfides as the initial products of supergene oxidation, Copiapó mining district, northern Chile. *American Mineralogist*, **54**: 1684–1710.
- Siuda, R., Gołębiowska, B., 2011.** New data on supergene minerals from Miedzianka-Ciechanowice deposit in the Rudawy Janowickie Mountains (Lower Silesia, Poland) (in Polish with English summary). *Przegląd Geologiczny*, **59**: 226–234.
- Siuda, R., Kruszewski, Ł., 2006.** New data on bayldonite, cornwallite, olivenite and philipsburgite from Miedzianka (Rudawy Janowickie Mts., Sudetes, Poland). *Mineralogia Polonica, Special Papers*, **28**: 202–204.
- Siuda, R., Kruszewski, Ł., 2013.** Recently formed secondary copper minerals as indicators of geochemical conditions in an abandoned mine in Radzimowice (SW Poland). *Geological Quarterly*, **57** (4): 583–600.
- Siwecki T., 2017.** Copper mineralization in agates from Sokolowiec (in Polish with English summary). M.Sc. Thesis, AGH.
- Sun, S., Konhauser, K., Kappler, A., Li, Y.L., 2015.** Primary hematite in Neoproterozoic oceans. *GSA Bulletin*, **127**: 850–861.
- Swęd, M., Urbanek, P., Krechowicz, I., Dworcak, P., Wiecka, P., Mlecza, M., Tobys, P., 2015.** Mineralogy of weathering heaps in the Miedzianka deposits (Holy Cross Mountains) (in Polish with English summary). *Przegląd Geologiczny*, **63**: 363–372.
- Sylwestrzak, H., 1972.** Geochemistry of uranium in the young Palaeozoic volcanicrocks of Lower Silesia basing on their general geochemical differences. *Biuletyn Państwowego Instytutu Geologicznego*, **259**: 5–92.
- Szopa, K., Krzykowski, R., Banasik, K., Król, P., Skreczko, S., Mounteanou, S.A., Koziarska, M., 2021.** EMPA, XRD, and Raman characterization of Ag-bearing djurleite from the Lubin Mine, Lower Silesia, Poland. *Minerals*, **11**, 454.
- Tadic, M., Trpkov, D., Kopanja, L., Vojnovic, S., Panjan, M., 2019.** Hydrothermal synthesis of hematite (α -Fe₂O₃) nanoparticle forms: synthesis conditions, structure, particle shape analysis, cytotoxicity and magnetic properties. *Journal of Alloys and Compounds*, **792**: 599–609.
- Vlasáč, J., Ferenc, Š., Mikuš, T., Polák, L., Luptáková, J., Biroň, A., 2018.** Occurrence of Cu sulphidic mineralization in the Permian basalts of Hronicum Unit at Banská Bystrica (Slovak Republic) (in Czech with English summary). *Bulletin Mineralogie Petrologie*, **26**: 176–187.
- Wieser, T., Žabiński, W., 1986.** Copper arsenate and sulphate minerals from Miedzianka near Kielce (Poland). *Mineralogia Polonica*, **17**: 17–42.
- Wodzicki, A., Piestrzyński, A., 1994.** An ore genetic model for the Lubin-Sieroszowice mining district, Poland. *Mineralium Deposita*, **29**: 30–43.
- Wojewoda, J., Mastalerz, K., 1989.** Climate evolution, allo- and autocyclity of sedimentation: an example from the Permo-Carboniferous continental deposits of the sudetes, SW Poland (in Polish with English summary). *Przegląd Geologiczny*, **37**: 173–179.
- Yuan, F., Jiang, S.Y., Liu, J., Zhang, S., Xiao, Z., Liu, G., Hu, X., 2019.** Geochronology and geochemistry of uraninite and coffinite: insights into ore-forming processes in the pegmatite-hosted uraniferous province, North Qinling, Central China. *Minerals*, **9**, 552.
- Zimnoch, E., 1978.** Ore mineralization of the Miedzianka deposit in the Sudetes (in Polish with English summary). *Biuletyn Instytutu Geologicznego*, **308**: 91–134.